Diagnostic accuracy of MRI techniques for treatment response evaluation in patients with brain metastasis

Teunissen, Wouter H.T.; Govaerts, Chris W.; Kramer, Miranda C.A.; Labrecque, Jeremy A.; Smits, Marion; Dirven, Linda; van der Hoorn, Anouk

Published in:
Radiotherapy and Oncology

DOI:
10.1016/j.radonc.2022.10.026

Publication date:
2022

Radiotherapy and Oncology 177 (2022) 121–133

Contents lists available at ScienceDirect

Radiotherapy and Oncology

journal homepage: www.thegreenjournal.com

Original Article

Diagnostic accuracy of MRI techniques for treatment response evaluation in patients with brain metastasis: A systematic review and meta-analysis

Wouter H.T. Teunissen [a,b,h], Chris W. Govaerts [d], Miranda C.A. Kramer [g], Jeremy A. Labrecque [c], Marion Smits [a,b,h], Linda Dirven [e,f], Anouk van der Hoorn [d,*]

[a] Erasmus MC, department of Radiology and Nuclear Medicine, Rotterdam, the Netherlands; [b] Brain Tumor Centre, Erasmus MC Cancer Institute, Rotterdam, the Netherlands; [c] Erasmus MC, Netherlands Institute for Health Science (NIHES), Rotterdam, the Netherlands; [d] University Medical Center Groningen, Medical imaging center, department of Radiology, Groningen, the Netherlands; [e] Leiden University Medical Center, department of Neurology, Leiden, the Netherlands; [f] Haaglanden Medical Center, department of Neurology, The Hague, the Netherlands; [g] University Medical Center Groningen, department of Radiotherapy, Groningen, the Netherlands; [h] Medical Delta, Delft, The Netherlands

ARTICLE INFO

Article history:
Received 11 May 2022
Received in revised form 11 October 2022
Accepted 21 October 2022
Available online 28 October 2022

Keywords:
Brain metastasis
Treatment response
Meta-analysis
MRI
Pseudoprogression

ABSTRACT

Background: Treatment response assessment in patients with brain metastasis uses contrast enhanced T1-weighted MRI. Advanced MRI techniques have been studied, but the diagnostic accuracy is not well known. Therefore, we performed a metaanalysis to assess the diagnostic accuracy of the currently available MRI techniques for treatment response.

Methods: A systematic literature search was done. Study selection and data extraction were done by two authors independently. Meta-analysis was performed using a bivariate random effects model. An independent cohort was used for DSC perfusion external validation of diagnostic accuracy.

Results: Anatomical MRI (16 studies, 726 lesions) showed a pooled sensitivity of 79% and a specificity of 76%. DCE perfusion (4 studies, 114 lesions) showed a pooled sensitivity of 74% and a specificity of 92%. DSC perfusion (12 studies, 418 lesions) showed a pooled sensitivity was 83% with a specificity of 78%. Diffusion weighted imaging (7 studies, 288 lesions) showed a pooled sensitivity of 67% and a specificity of 79%. MRS (4 studies, 54 lesions) showed a pooled sensitivity of 80% and a specificity of 78%. Combined techniques (6 studies, 375 lesions) showed a pooled sensitivity of 84% and a specificity of 88%. External validation of DSC showed a lower sensitivity and a higher specificity for the reported cut-off values included in this metaanalysis.

Conclusion: A combination of techniques shows the highest diagnostic accuracy differentiating tumor progression from treatment induced abnormalities. External validation of imaging results is important to better define the reliability of imaging results with the different techniques.

Brain metastasis are the most common intracranial malignant tumors with a high mortality rate[1]. Although treatment for the primary tumor may also have an effect on brain metastasis (e.g. immunotherapy), the most important treatment of brain metastasis is high dose focal radiation therapy, while surgical resection is also an option in selected patients[2]. Magnetic resonance imaging (MRI) of the brain is the common radiological modality to monitor treatment effect during follow-up.

One of the major radiological challenges in patients with brain metastasis treated with focal high dose radiation therapy is the differentiation between tumor progression (PD) and treatment induced radiological abnormalities, also called pseudoprogression (PsP). This phenomenon is called radiation necrosis when occurring (late) after radiation therapy only[3]. Conventional T2-weighted and contrast-enhanced T1-weighted MRI techniques are considered unreliable to differentiate between PD and PsP[4]. Therefore, advanced MRI techniques such as diffusion weighted imaging (DWI) and perfusion weighted imaging (PWI) can be added to the scanning protocol to assist in differentiating PD and PsP. PWI is an umbrella term that encompasses different available perfusion MRI techniques: dynamic susceptibility contrast (DSC), dynamic contrast enhanced (DCE) and arterial spin labelling (ASL). DSC measures T2-weighted or T2*-weighted signal changes over time after administration of an exogenous gadolinium based contrast agent (GBCA). DCE measures T1-weighted signal changes over time after administration of exogenous GBCA, while ASL uses magnetically labelled blood to measure blood flow without the

* Corresponding author at: Medical imaging center, department of Radiology, PO Box 30.001, 9700 RB, Groningen, the Netherlands.
E-mail address: a.van.der.hoorn@umcg.nl (A. van der Hoorn).

https://doi.org/10.1016/j.radonc.2022.10.026
0167-8140/

need of exogenous contrast. The ability to accurately distinguish between PD and PsP after focal high dose radiation therapy for brain metastasis has important clinical implications for patients and clinicians. In case of PD switch to a different treatment or re-irradiation might be indicated while in case of PsP the current treatment can be judged as effective and should be continued.

Multiple studies have determined the sensitivity and specificity of the available (advanced) MRI techniques in the assessment of brain metastasis treatment response, but patient numbers are usually small and studies are heterogeneous in terms of patient population and imaging techniques, warranting pooling of data to obtain more reliable results. Also, previous reviews did not include all available MRI techniques [5]. There is a wide variety in the use of different (advanced) MRI techniques in current daily clinical practice. Dynamic susceptibility contrast (DSC) perfusion is currently the most commonly used perfusion MRI technique to differentiate between PD and PsP based on a relative cerebral blood volume (rCBV)[6]. However, the optimum rCBV value for differentiating between PD and PsP is unknown and there is a lack of external validation of the reported thresholds [7]. This external validation is a requirement for the generalisability of such thresholds.

The aim of this systematic review and meta-analysis was to provide an up to date overview of the current MRI techniques and their diagnostic accuracies for monitoring the response of treated brain metastasis, focusing on advanced MRI techniques like PWI, DWI, and spectroscopy. The main research question was to investigate which MRI technique has the best sensitivity and specificity to distinguish PD from treatment induced abnormalities during follow-up in brain metastasis patients. In addition, we performed an external validation of the various reported cut-off values for DSC perfusion in an independent patient cohort. This will provide insight into the generalisability of rCBV cut-off values that can be used in the clinic or further research.

Methods

The systematic review and meta-analysis were performed according to the Preferred Reporting Items for Systematic Reviews and Meta-Analysis (PRISMA) criteria [8]. In addition, the Cochrane handbook for review of diagnostic test accuracy and the AMSTAR guidelines for the assessment of the methodological quality of systematic reviews were used [9]. This review and meta-analysis was not registered in a register.

Search strategy

The search strategy was designed under the supervision of information specialists of the Erasmus MC Medical Library, Rotterdam, The Netherlands. The database search was conducted in Embase, Medline, Web Of Science, Cochrane and Google Scholar. We used the following keywords: brain metastasis, radiation therapy, treatment response, MRI, perfusion MRI, diffusion MRI, MR spectroscopy, chemical exchange saturation transfer (CEST) and blood oxygenation level dependent (BOLD) imaging. The full details on the search strategy can be found in the supplementary material. The first search was performed on May 1st 2020 and updated on November 8th 2021. There were no limits regarding the year of publication.

Selection criteria

Studies eligible for inclusion consisted of patients with intra-axial brain metastasis of extracranial primary cancer treated with focal (high dose) radiation therapy. Treatment response had to be evaluated by MRI, i.e. conventional and/or advanced MRI. The definitive diagnosis, on either treatment induced abnormalities or true tumor progression, was assessed by histopathological assessment of resected tissue, imaging follow-up, clinical follow-up or a combination of these. All consecutive series of patients, both retrospective and prospective, were included. Case reports, case series and (systematic) reviews were excluded. Only articles written in English were considered. Studies were included for meta-analysis if information for the 2×2 tables could be extracted. The 2×2 tables were populated with the numbers of true positive (TP), true negative (TN), false positive (FP) and false negative (FN) MRI-based diagnoses. We defined true progression as the presence of disease and radiation induced abnormalities as absence of disease.

Study selection, data extraction and quality assessment

After deduplication of the identified articles, two independent reviewers (WT, CG) screened all titles and abstracts according to the predefined selection criteria. A third reviewer (AH) was consulted in case of discrepancies. In the same way, full text screening was performed by the two independent reviewers. To limit possible publication bias, conference abstracts were considered for data extraction if sufficient information was available.

A data extraction form was used to systematically extract the general study information (i.e. study design, total number of included patients, mean age, gender, primary tumor type, MRI characteristics and type and timing of follow-up) as well as numbers of TP, FP, TN and FN. 2×2 tables were made per imaging technique. If more than one technique was used and authors provided TP, FP, TN and FN for a combination of techniques, these were used in the pooled analysis for the 'combined techniques group'. Authors were contacted for further information if the data for the 2×2 table could not be extracted. If no further information could be provided or the authors did not respond, these studies were excluded for data extraction and not further considered. To perform the external validation, thresholds to distinguish PD from PsP were additionally extracted in studies reporting DSC techniques.

The risk of bias was assessed according to the quality assessment of diagnostic accuracy studies (QUADAS-2), consisting of the following domains: patient selection, index test, reference standard, flow and timing [10]. Data extraction and quality assessment were performed by the same two independent reviewers (WT, CG) and discrepancies were resolved by a third reviewer (AH). No studies were excluded from the analyses based on the QUADAS-2 assessment.

Statistical analysis

To provide a graphical overview of the results of the included studies and their results per MRI technique, forest plots were created with RevMan 5.4.1 (Cochrane collaboration, Copenhagen, Denmark). Pooled sensitivity and specificity for all studies were calculated with the "MADA package" in Rstudio [11]. As heterogeneity between the studies was expected, a random effects model was used to calculate pooled sensitivities and specificities for each MRI technique [12]. For an overview of the pooled data and their heterogeneity per imaging technique, summary receiver operating characteristic (SROC) curves were made.

External validation of DSC perfusion MRI

The rCBV ratio thresholds reported in the studies describing DSC were validated in an external data set, consisting of a retrospective convenience sample of 39 patients with brain metastasis from the Erasmus MC. This external validation study was reviewed

by the Erasmus MC Medical Ethics Committee and all patients had either provided written informed consent or were already deceased at the time of inclusion. All patients had undergone follow-up with 1.5 or 3 T MRI including DSC perfusion with a preload bolus between 2013 and 2019. All patients had received focal high dose radiation therapy. Final diagnosis, PD or PsP, was determined by histopathology (n = 5) or follow-up imaging (n = 34) with mean follow-up time of 5.4 months. rCBV maps were computed with Intellispace Portal (Philips Healthcare) using leakage correction. First, a region of interest (ROI) of at least 70 mm^2 was drawn manually in a representative part of the tumor and subsequently copied to the contralateral normal appearing white matter (NAWM). Then, the mean tumor values and mean NAWM values were used to calculate the ratios between tumor and NAWM. Sensitivity and specificity values were calculated for each threshold identified in the systematic review.

Results

Selection and general description of studies

After deduplication, a total of 8318 unique titles were identified through our electronic database search (see Fig. 1 for the flowchart). After screening titles and abstracts, 245 studies were deemed eligible for full text screening. This resulted in the identification of 53 possibly relevant studies. From 37/53 studies, data for the 2 × 2 tables could be extracted, making them eligible for quantitative analysis (see Table 1 for study characteristics). Characteristics of the sixteen studies[13–28] which could not be included are shown in supplementary table 1. Patient and imaging characteristics between studies included or not included in the quantitative analysis did not differ (see Table 1 and supplementary table 1).

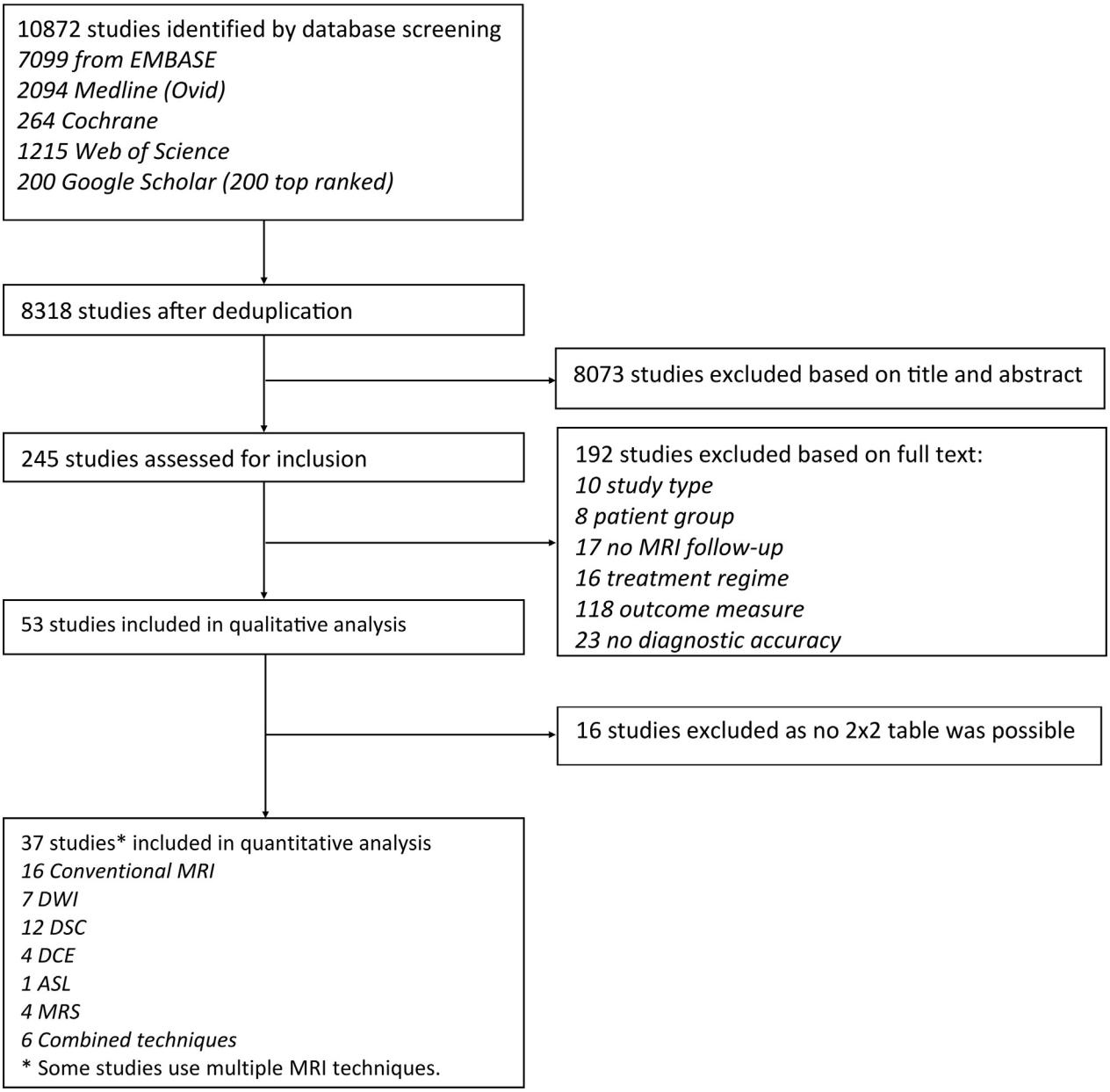

Fig. 1. Flow chart of included studies.

Table 1
Characteristics of included studies.

Reference	N (pt)	N (lesions)	Study type	Age (yr.) mean ± SD (range)	M/F	Histology primary tumour	RT technique	RT schedule (Gy)	Time point MRI	Reference standard†	Index test	MRI details	Diagnostic accuracy cut-off
Barajas et al. [29]	27	34‡	retro	-	11/16	A,B,C,D,F	GK	-	3 months	histology (65 %) radiology (35 %)	DSC	1.5 T	rCBV ratio 1.54
Cha et al. [62]	16	16	retro	56 (38–71)	9/7	A,B,C,D,F	SRS nos	-	-	histology (100 %)	DWI	3 T. b-values (b = 0, 1000 s/mm2)	-
											DSC	3 T	rCBV ratio 2.6
											DWI + DSC	-	-
Chernov et al. [15]	9	9	retro	54 (30–84)	5/4	A,D,F,G	GK	-	-	-	MRS	Multi voxel MRS. Metabolites: Cho, Cr, NAA, Lac, Lip.	-
Choi et al. [31]*	29	38‡	retro	-	-	-	SRS nos	-	-	-	DCE	bimodal histogram parameters of wash-in – Emax. ratio	-
Cicone et al. [57]	42	37‡	retro	64 (38–84)	19/23	C,D,E,F,G	LIN	1x18-22 or 3x9	>2 months	radiology (100 %)	DSC-rCBV	1.5 T	-
Cicone et al. [41]	30	34	retro	63 (37–83)	13/17	C, D, E, F	SRS nos	1x16-22 or 3x9	3 or 6 months	radiology (100 %)	Conventional	-	-
Correa et al. [40]*	-	37	retro	-	-	-	SRS nos	-	-	histology (100 %)	Conventional	Lesion habitat sub-compartments	-
Dequesada et al. [32]	31	12‡	retro	-	-	-	LIN	-	-	-	Conventional	Lesion quotient	<0.3 > 0.6
Detsky et al. [42]	9	10‡	retro	-	-	-	SRS nos	1x18-20 or 5x5.5–7	-	-	DWI ADC	b-values (b = 0, 200, 400, 600, 800, 1000 s/mm2)	-
Dohm et al. [48]	73	78	retro	54 (16–88)	27/46	B,C,D,E,F	GK	-	1–3 months	histology (100 %)	Conventional	CaPTk radiomics features	-
Hainc et al. [49]	59	59	retro	59 (40–80)	23/36	G, D, E, F	SRS nos	1x10-27 (mean 18)	-	histology (100 %)	DWI	1.0.5, 3 T, b-values (b = 0, 1000 s/mm2)	-
Hatzoglou et al. [43]	26	26	pros	63 (24–81)	-	C,D,E,F	SRS nos	1X15-21	Median 9 months	histology (25 %) radiology (75 %)	DCE-Ktrans	1.5, 3 T	Ktrans ratio ≥ 3.6
Hettal et al. [53]	20	20	retro	57 (27–78)	10/10	D,E,F,G	CK	3x9	Average 10.5 months	radiology (100 %)	Conventional	1.5, 3 T, 1766 radiomics features	-
Hoefnagels et al. [58]	31	34‡	retro	54 (32–72)	12/19	D,E,F,G	SRS nos	1x18-24	3 months	histology (18 %) radiology (82 %)	DSC-rCBV	1.5 T	2.0 rCBV ratio (NAWM)
Huang et al. [59]	33	24‡	retro	63(57–79) PsP 56(38–68)PD	13/20		GK	1x15-21	16(2–33) months	histology (12 %) radiology (88 %)	MRS	1.5 T metabolites: Cho, Cr, NAA	1.2 Cho/nCho
		27‡ 33									DSC-rCBV	1.5 T	2.0
											Conventional	1.5 T T1/T2 volume	-
Kano et al. [44]	68	44‡	retro	55(24–81)	33/35‡	B,C,D,E,F	SRS nos	-	-	histology (100 %)	Conventional	T1/T2 match and mismatch	-
Kim et al. [33]	91	91	retro	51.5 ± 8.5 (PsP)	46/45	D,F,G	GK	1x17.5 ± 0.7	-	-	DWI (IVIM)	3 T. b-values (0, 10, 20, 40, 60, 80, 100, 120, 140, 160, 180, 200, 300, 500, 700,	-

Table 1 (*continued*)

Reference	N (pt)	N (lesions)	Study type	Age (yr.) mean ± SD (range)	M/F	Histology primary tumour	RT technique	RT schedule (Gy)	Time point MRI	Reference standard†	Index test	MRI details	Diagnostic accuracy cut-off
				47.4 ± 6.7 (PD)								and 900 s/mm2)	
											DSC (rCBV) + DWI (ADC)	3 T DSC	-
											DSC (rCBV) + DWI (IVIM)		-
Knitter et al. [54]	29	32‡	retro	56 (48–64.5)	10/19	D,R,F,G	LIN	1x18-24	2–3 months post SRS, then every 3 months	radiology (100 %)	DSC – rCBV	3 T/1.5 T	-
											DCE – Ktrans		-
											DWI (ADC)	b values (b = 0, 1000 s/mm2)	-
Koh et al. [34]	72	72	retro	48.1 ± 9.3 (PS) 50.5 ± 8.9 (PsP)	42/30	-	GK	1x17.5 ± 0.9 (PD) 1x17.2 ± 0.7 (PsP)	< 3 months	histology (18 %) radiology (82 %)	DWI (ADC)	3 T, b = 0, 1000 s/mm2	-
											DWI + DSC		-
											DWI + DCE	time, 6 min and 45 s.	-
											DWI + DSC + DCE		-
Lai et al. [35]	14	14	retro	61(46–79)	9/5	B,C,D,E,F	SRS nos	1x16-22 or 3x9	7.5 (3–12) months	histology (100 %)	ASL	pseudo continuous labeling spin-echo sequence. PLD = 1.5 sec.	-
Larroza et al. [55]	73	55‡	retro	56.8 ± 10.3	37/36	-	SRS nos	1 × 20 (median)	Every 3 months	Histology (10 %) radiology (90 %)	Conventional	1.5 T	-
Lee et al. [50]	76	69‡	retro	57.9 (31–87)	34/42	A-F	SRS nos	29.8 ± 11.2 (PD) 31.0 ± 13.5 (PsP)	2–3 months	Histology (14 %) radiology (86 %)	CE-T1 + DWI + DSC	3 T	-
Leeman et al. [45]	49	48‡	retro	58(29–83)	30/19	D,E,F,G	CK, TRI	1 × 20.5 (median)	10 (0.7–63) months	histology (100 %)	Conventional		-
Lohmann et al. [46]	52	52	retro	55(17–75)	13/39	D,E,F,G	SRS nos	-	15 (3–64) months	histology (37 %) radiology (63 %)	Conventional	42 radiomics features	-
Mitsuya et al. [64]	27	28	pros	59.6 (38–85)	14/13	A,B,D,F	SRS nos, LIN, GK, CK	1x10-30	Every 1–3 months	histology (7 %) radiology (93 %)	DSC-rCBV	1.5 T	2.1
Muto et al. [47]	29	78	retro	53(33–79)	11/18	D,F,G	SRS nos	18–30	45 days and 3 months	histology (10 %) radiology (90 %)	DSC-rCBV	1.5 T	2.1
Narloch et al. [36]	34	30‡	retro	52.5 (22–71)	16/18	D,E,F,G	SRS nos	1x11.2–27.7	Every 3 months	histology (100 %)	Conventional	-	-
Otman et al. [52]	15	15	retro	64.4 ± 8.7	6/9	G, D	SRS nos	-	3 months	histology (53 %) radiology (47 %)	Conventional	3 T	-
Peng et al. [56]	66	82	retro	56.5 (29–86)	-	B,C,D,E,F	LIN, GK, CK	14–25 (mean 20)	302 (21–1351) days	histology (94 %) radiology (6 %)	Conventional	51 radiomics features	-

(*continued on next page*)

Table 1 (*continued*)

Reference	N (pt)	N (lesions)	Study type	Age (yr.) mean ± SD (range)	M/F	Histology primary tumour	RT technique	RT schedule (Gy)	Time point MRI	Reference standard†	Index test	MRI details	Diagnostic accuracy cut-off
Sawlani et al. [60]	6	6	retro	-	-	C,D,E	CK	1x18-21	Every 3 months	histology (-) radiology (-)	DWI-ADC	3 T. No b-values mentioned.	$\leq$ 1000x 10^{-6} mm^2/s
											DSC-rCBV		2.1
											MRS	Metabolites: NAA, Cr, Cho, Lip	1.8
Stockham et al. [4]	51	46‡	retro	57 (28–73)	23/28	B,C,D,E,F	GK	1x18-24	-	histology (100 %)	Conventional	1 T, 1.5 T, 3.0 T. Lesion quotient	<0.3 (PsP) > 0.6 (PD)
Tomura et al. [37]	15	18	retro	63.3 ± 10.9	9/6	D,F,G	GK, CK	1x18-32	-	histology (100 %)	DWI-ADC	No b-values mentioned.	-
											DCE-CER		-
Travers et al. [51]	20	15‡	retro	60	-	A, C,D,E,F	LIN	15–30	3 months	histology (100 %)	MRS	3 T, single voxel,	-
Truong et al. [38]	32	12‡	retro	53 (38–84)	12/20	C,D,E,F	GK	1x14-32	First 2 months, than every 3 months	histology (100 %)	DSC-rCBV		-
		9‡									MRS	Metabolites: Cho, Cr, NAA, Lip, Lac	-
Wang et al. [39]	56	56	retro	59 (31–80)	26/30	D,F,G	GK	1x18-21	Every 3 months	radiology (100 %)	DSC-rCBV	3 T	1.74
											Conventional	3 T. $T1_{5min}$ and $T1_{60min}$	673.6 and 1086.0 ms
Wang et al. [63]	46	58	retro	61(52–69) PD 62(56–68) PsP	24/22	D,F,G	GK	1x17-23	Every 3 months	Histology (8 %) radiology (92 %)	DSC-absolute CBV	3 T	21.8 ml/100 g
Zhang et al. [61]	84	84	retro	28–79	46/38	D,E,F,G	GK	1x13-24	-	radiology (100 %)	Conventional	1.5 T 2280 radiomics features. concordance correlation coefficients (CCCs)	CCC > 0.7 PD CCC −0.1–0.1 PsP

A: lung adenocarcinoma, B: SCLC, C: NSCLC, D: breast cancer, E: melanoma, F: other, G: lung not specified. †percentage shows proportion of patients with histopathological and radiological confirmation, if available.
RT techniques: SRS nos: stereotactic radiosurgery not otherwise specified, LIN: LINAC-based SRS, GK: Leksell Gamma Knife® (Elekta Instruments), CK: Cyber Knife Radiosurgery System® (Accuray), TRI: Trilogy Radiosurgery System (Varian Medical Systems).

* Abstract.

‡ Subset of lesions used for analysis.

Table 2
Pooled estimates of sensitivity and specificity of the 50 included 2 × 2 tables per MRI modality. *Pooled analysis for ASL was not possible as there was only one eligible study.*

Imaging technique	No. of 2 × 2 tables	No. of lesions	Pooled sensitivity (95 % CI)	Pooled specificity (95 % CI)
Conventional	16	726	0.79 (0.70–0.86)	0.76 (0.65–0.84)
DCE PWI	4	114	0.74 (0.61–0.84)	0.92 (0.81–0.97)
DSC PWI	12	418	0.83 (0.73–0.89)	0.78 (0.65–0.88)
DWI	7	288	0.67 (0.55–0.78)	0.79 (0.65–0.88)
MRS	4	54	0.80 (0.34–0.97)	0.78 (0.39–0.95)
Combined techniques	6	375	0.84 (0.78–0.89)	0.88 (0.77–0.94)

A total of 50 2 × 2 tables from the eligible studies (comprising 1989 lesions; Table 2) could be created for the quantitative analysis, because some studies reported on more than one MRI technique. The vast majority (35/37) of the analyzed studies had a retrospective study design; only two studies had a prospective design. Sixteen authors were contacted for more information because information for a 2 × 2 table could not be extracted, which resulted in one extra 2 × 2 table. The other authors did not respond (75 %) or could not provide this extra information (19 %).

Methodological quality of the included studies

According to the first domain of the QUADAS-2 criteria, shown in supplementary Fig. 1.A, patient selection showed a high risk of bias in 12 out of 37 studies [29–40]. Some of these studies used selection criteria which could induce bias, such as excluding patients who used dexamethasone or showed clinical deterioration [33,34]. One study excluded patients with lesions which could induce susceptibility artefacts such as metastasis from melanoma [29]. In the index test domain, 16 out of 37 studies showed a high risk of bias, because for these studies it was unknown if the results of the index test were interpreted with or without knowledge of the reference test [30,35,36,40–52]. Also, in many studies (n = 17), a predefined cut-off value of the index test was missing [30,31,33–38,41,42,44–46,53–56]. In the reference test domain, 9 out of 37 studies showed a high risk of bias [30,31,33,37,47,50–52,57], mainly because of the choice of the reference test. In the flow and timing domain, 17 out of 37 studies showed a high risk of bias[4,30–33,36–38,41,42,44,45,51,52,56,58,59], which was mostly due to the fact that it was not always clear if all patients had the same reference test. It was also not always clear what the timing of the reference test was. Only 9 out of 37 studies [39,51–55,60–62] did not show a high risk of bias in any of the four QUADAS-2 domains. We had some concerns regarding the applicability assessment of one study [29], in which scans with severe susceptibility artefacts were excluded, even though these are common in daily clinical practice. Supplementary Fig. 1.B shows the clustered bar graphs of quality assessment of the included studies and provides a quick overview of the QUADAS-2 assessment.

Diagnostic accuracy

We identified sixteen studies using conventional MRI [4,32,36,39,40,44–46,48,52,53,55–57,59,61]. Besides anatomical images, all conventional MRI studies used additional analytical techniques (such as radiomics features). Seven studies used DWI [33,34,37,42,49,54,60], twelve DSC perfusion MRI [29,38,39,41,47,54,58–60,62–64], four dynamic contrast enhanced (DCE) perfusion MRI [31,37,43,54], four magnetic resonance spectroscopy (MRS) [30,51,59,60], and one study used arterial spin labelling (ASL) perfusion MRI [35]. Lastly, six data sets (five derived from three studies and one separate study) used combined MRI techniques to calculate sensitivity and specificity [33,34,50,62].

Forest plots for each MRI technique with information on the sensitivity, specificity and true and false positives / negatives rates are shown in Fig. 2. The pooled results of the meta-analyses are shown in Table 2. SROC curves are shown in Fig. 3.

Conventional MRI

Forest plots of conventional MRI (16 studies, 726 lesions) showed a wide variation in reported sensitivities, ranging from 50 % to 100 %, and a wide variation in reported specificities, ranging from 15 % to 94 %. Four studies were outliers, with low reported specificities of 15–58 % [32,36,57,61]. The calculated heterogeneity (I^2) of the included studies was 99.5, indicating considerable heterogeneity. Overall, pooled sensitivity was 0.79 (95 % CI: 0.70–0.86) and pooled specificity 0.76 (95 % CI: 0.65–0.84).

DCE perfusion

Forest plots of DCE perfusion (4 studies, 114 lesions) showed that the sensitivity ranged between 56 % and 80 %, while the specificity was fairly similar across studies, ranging between 88 % and 96 %. The calculated heterogeneity (I^2) of the included studies was 98.9, indicating considerable heterogeneity. Overall, DCE perfusion had a pooled sensitivity of 0.74 (95 % CI: 0.61–0.84) and specificity of 0.92 (95 % CI: 0.97–0.81).

DSC perfusion

Forest plots of DSC perfusion (12 studies, 418 lesions) showed both heterogeneous sensitivity and specificity values, ranging between 56–100 % and 0–100 % respectively. Two studies [38,60] in particular showed large confidence intervals and one of them [38] showed a specificity of 0 %, possible due to the low sample sizes ($N \leq 12$). The calculated heterogeneity (I^2) of the included studies was 99.3, indicating considerable heterogeneity. Overall, DSC perfusion had a pooled sensitivity of 0.83 (95 % CI: 0.73–0.89) and specificity of 0.78 (95 % CI: 0.65–0.88).

Eight of the 12 DSC studies [29,39,47,58–60,62,64] mentioned a specific rCBV threshold ranging between 1.54 and 2.6 (median 2.05). In 6 out of 8 studies this threshold was derived from the original dataset, while two studies used pre-defined rCBV ratios based on thresholds mentioned in literature [47,60].

DWI

Forest plots of DWI (7 studies, 288 lesions) showed heterogeneous sensitivity and specificity values with wide confidence intervals, between 30–100 % and 60–100 %, respectively. The calculated heterogeneity (I^2) of the included studies was 98.9, indicating considerable heterogeneity. Overall, DWI had a pooled sensitivity of 0.67 (95 % CI: 0.55–0.78) and specificity of 0.79 (95 % CI: 0.65–0.88).

MRS

Forest plots of MRS (4 studies, 54 lesions) also showed wide confidence intervals for all studies. Reported sensitivity was 100 % in three studies [30,51,60] and 32 % in one study [59]. Reported specificity was high for three studies [30,59,60] and low for one study [51]. There were too few studies to calculate a reliable I^2. Overall, MRS had a pooled sensitivity of 0.80 (95 % CI: 0.34–0.97) and specificity of 0.78 (95 % CI: 0.39–0.95).

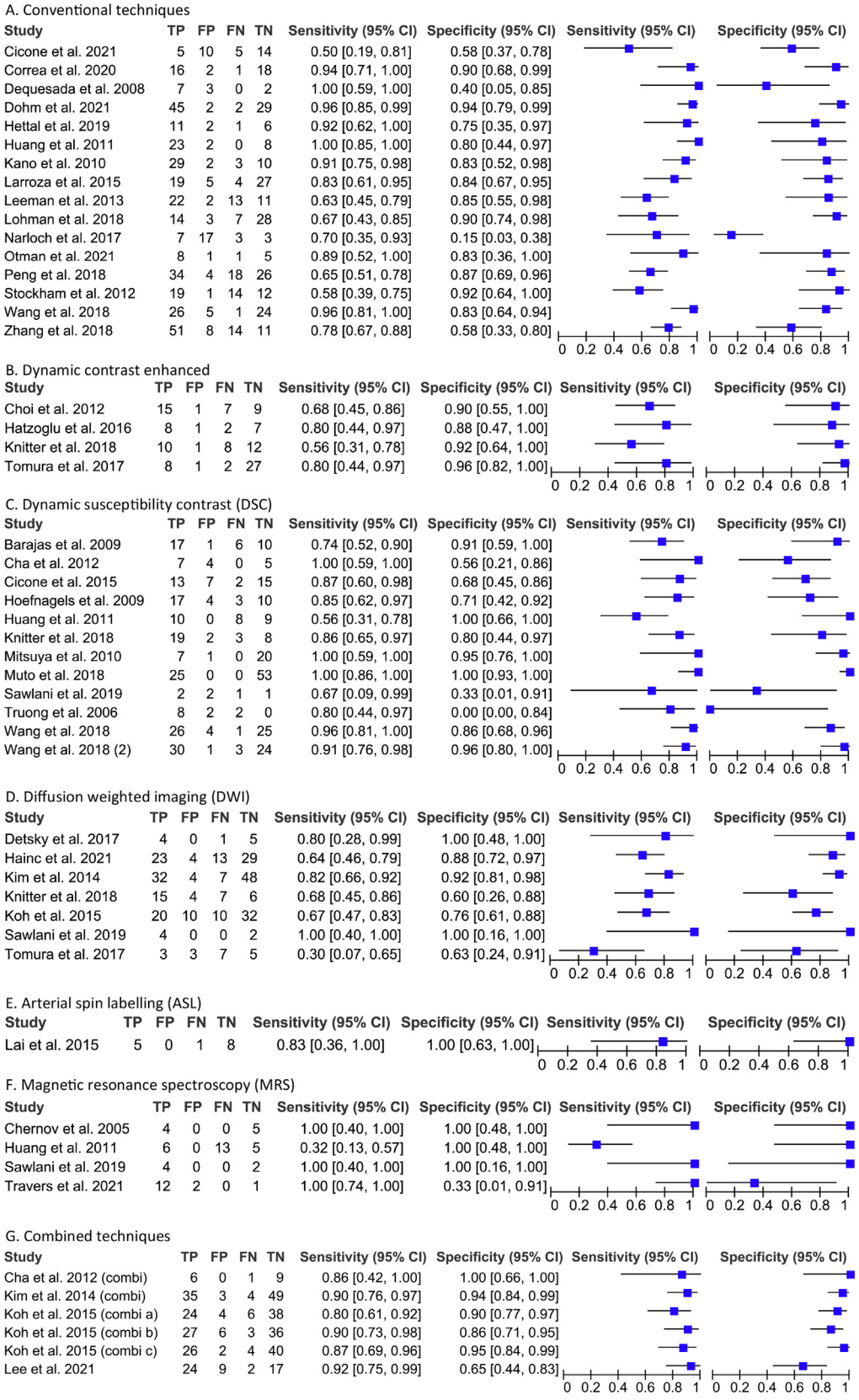

Fig. 2. Forest plots with the diagnostic accuracy of the different MRI techniques that were analyzed. TP: true positive, FP: false positive, FN: false negative, TN: true negative, CI: confidence interval.

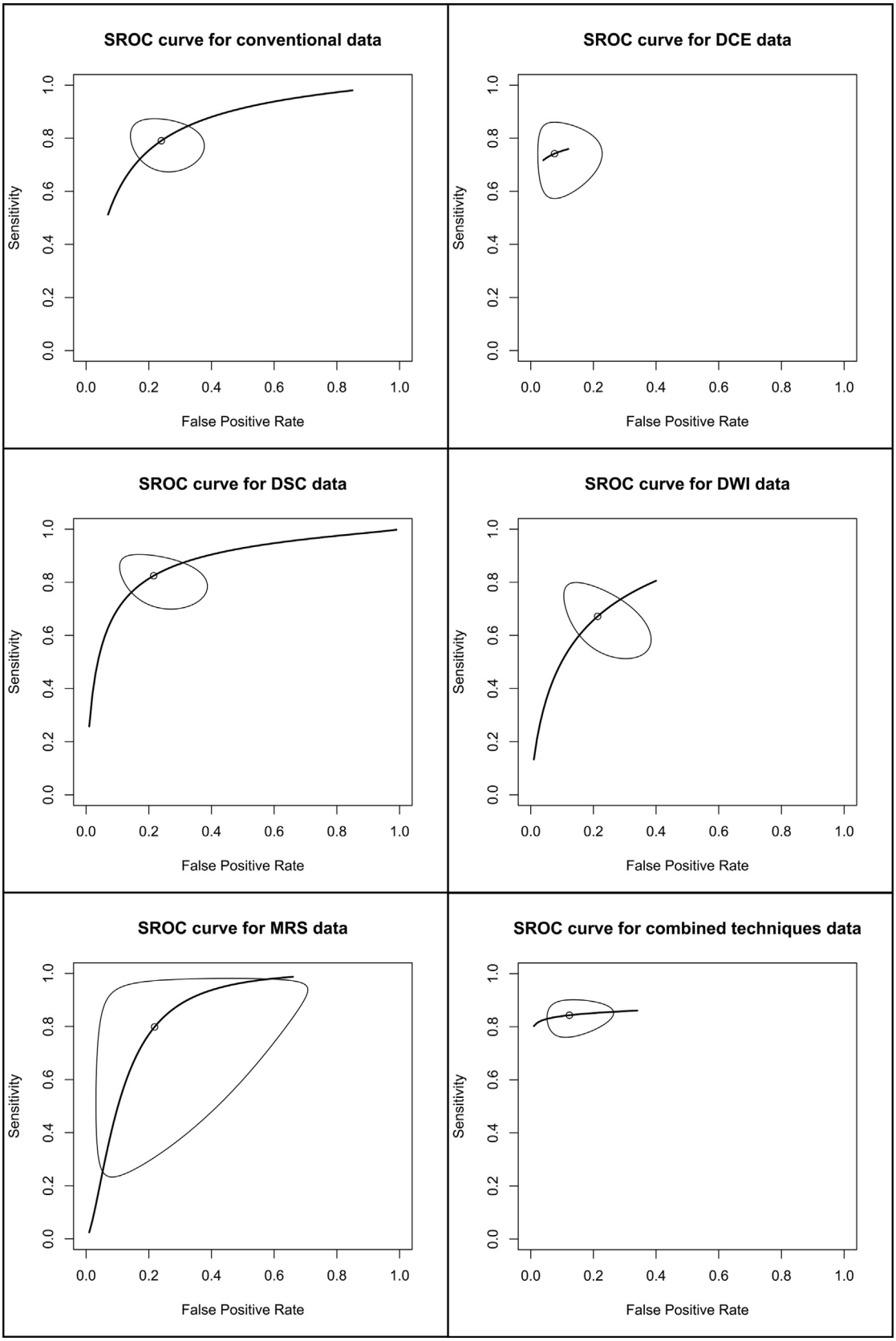

Fig. 3. SROC curves for conventional MRI, DCE, DSC, DWI, MRS and combined techniques.

Table 3
Included DSC perfusion studies with rCBV thresholds.

Reference	rCBV threshold	Reported study data						External validation					
		TP	FP	TN	FN	Sensitivity	Specificity	TP	FP	TN	FN	Sensitivity	Specificity
Barajas et al. [29]	1.54	17	1	10	6	0.739	0.909	13	3	19	4	0.77	0.86
Cha et al. [62]	2.6	7	4	5	0	1.000	0.556	8	8	21	9	0.47	0.95
Hoefnagels et al. [58]	2.0	17	4	10	3	0.850	0.714	11	6	21	1	0.65	0.95
Huang et al. [59	2.0	10	0	9	8	0.556	1.000	11	6	21	1	0.65	0.95
Mitsuya et al. [64]	2.1	7	1	20	0	1.000	0.952	11	6	21	1	0.65	0.95
Muto et al. [47]	2.1	25	0	53	0	1.000	1.000	11	6	21	1	0.65	0.95
Sawlani et al. [60]	2.1	2	2	1	1	0.667	0.333	11	6	21	1	0.65	0.95
Wang et al. [39]	1.74	26	4	25	1	0.963	0.862	13	4	20	2	0.77	0.91

The columns below "Reported study data" describe the reported TP, FP, TN, FN, sensitivity and specificity of these eight studies. Below "External validation" TP, FP, TN, FN, sensitivity and specificity are calculated. These calculations are made by using the thresholds mentioned in the included studies, applied on an external data set of 39 patients with metastasis as described in the methods.

ASL

We found only one study using ASL [35], reporting a sensitivity of 0.83 (95 % CI: 0.36–1.00) and a specificity of 1.00 (95 % CI: 0.63 – 1.00).

Combined perfusion and diffusion techniques

Four studies reported data to construct six different 2 × 2 tables (375 lesions) [33,34,50,62], in which a combination of DWI and DSC perfusion was used. One of these studies [34] also used DWI with DCE perfusion and a combination of DWI, DSC and DCE. In addition, one study reported only a combination of techniques [50]. Forest plots of combined techniques all showed a high sensitivity (range: 86–92 %) and specificity (range: 65–100 %) with small confidence intervals. The calculated heterogeneity (I^2) of the included studies was 99.6, indicating considerable heterogeneity. Overall, the combination of techniques had a pooled sensitivity of 0.84 (95 % CI: 0.78–0.89) and specificity of 0.88 (95 % CI: 0.77–0.94).

External validation of DSC-rCBV thresholds

The mean age of patients included for external validation was 60.8 (standard deviation: 10.6) years and 21 out of 39 (54 %) patients were female. Twenty-five patients had brain metastasis from lung cancer, seven from breast cancer, three from melanoma and four patients with other cancers or unknown primary tumors. The reported rCBV thresholds of 1.5–2.6 have a sensitivity between 0.47 and 0.77 and specificity between 0.86 and 0.95 (Table 3) in our validation cohort. The previously determined threshold of 2.0–2.1 would be optimal based on the external validation.

Discussion

This systematic review and meta-analysis comprises 37 unique studies (resulting in 50 2 × 2 tables with relevant information) on the diagnostic accuracy of conventional and advanced MRI techniques for evaluating treatment response in patients with brain metastasis after focal high dose radiotherapy. We demonstrated that among the available advanced MRI techniques, DSC and DCE perfusion had the best diagnostic accuracy. Moreover, the combination of multiple perfusion and diffusion techniques outperformed the diagnostic accuracy of these techniques separately, with a pooled sensitivity of 0.84 and specificity of 0.88.

The findings in this meta-analysis in brain metastasis patients are consistent with the findings in comparable cohorts of patients with high grade glioma [65], in which similar values of sensitivity and specificity for conventional MRI, DWI, MRS, DSC and DCE perfusion were reported.

In general, if we compare the pooled sensitivities with specificities identified in this meta-analysis, slightly higher specificities were observed. The observed high specificity has important clinical implications, as it is relevant to identify those patients with PsP. If PsP occurs, this usually means that follow-up with MR imaging or systemic anti-tumor therapy will be continued, whereas PD usually means a switch or discontinuation of systemic anti-tumor treatment or that salvage radiation therapy will be administered.

Our results suggest that perfusion MRI and DWI as advanced MRI technique additional to conventional MRI have the best diagnostic performance. Although DWI is routinely used, PWI is used less frequently in clinical practice. Nevertheless, based on the currently available literature it might be worth considering to add PWI to conventional MRI in daily clinical practice for patients with an unclear treatment response on conventional imaging. These PWI results should subsequently be combined with the other sequences to draw a definite conclusion on the treatment response and thus the management of the patient. PWI could be done using a DSC, DCE or ASL technique of which DSC is most commonly performed. We showed that DCE and DSC have comparable diagnostic accuracy. The diagnostic accuracy of ASL remains largely unknown with only one study being available. However, ASL might be a promising technique to distinguish PD from PsP, because of the previously shown diagnostic accuracy in glioma [66]. Further research is thus warranted to assess its value in the context of brain metastasis. Moreover, DCE and ASL perfusion have several advantages over DSC perfusion, such as fewer issues with susceptibility artefacts and leakage effects. Furthermore, ASL has less issues with a tumor location near major blood vessels [67]. On the other hand, DSC is considered more easy to implement, resulting in it being currently the most commonly used technique. This meta-analysis focusses on MRI only, but positron emission tomography (PET) is also used to differentiate between PD and PsP. Different PET tracers can be used, such as 18F-2-fluoro-2-deoxy-D-glucose (FDG) and different amino acid PET tracers, such as methionine (MET). As described in a systematic review by Galldiks et al. from 2019 [68], studies on FDG PET show a lower diagnostic performance than MRI, while amino acid PET shows a high diagnostic performance. Nevertheless, amino acid PET scans are more expensive and less widely available compared to MRI.

This meta-analysis has several limitations. First, the quality of many included studies is some cases questionable, because of an unknown or high risk of bias. A large part of this high risk of bias was due to bias in selection of patients and performing the index test (e.g. lack of predefined cut-off values). For determining true and generalisable clinical value it is important to either use predefined cut-off values or to externally validate cut-off values determined within the study. Previous data [69] has shown that a considerable number of lesions are difficult to interpret due to their location or artifacts (15 %) or due to unmeasurable residual metastases (31 %). Exclusion of these patients may results in an overestimation of the value of perfusion MRI. Only one study reported excluding patients on the basis of susceptibility artefacts, but it is not certain whether other studies included in this meta-

analysis did or did not do the same. Another limitation is that not all possible eligible studies could be analysed because relevant information was lacking and could not be retrieved. Nevertheless, we believe that these missing results did not influence the results because the excluded studies were not different from the included studies with respect to imaging techniques and patient characteristics. Another limitation is the low number of studies using histopathology as the gold standard for determining the final diagnosis. Ideally, only studies with a histopathological diagnosis should be included, as histopathology is generally considered the gold standard, but this would limit the number of eligible studies. In addition, this would not reflect daily clinical practice, where information on histopathology is also not always available and would thus induce an inclusion bias. Through the mechanism of "diagnosis by indication" the use of histopathology tends to lead to a larger proportion of PD and the use of radiology to a larger proportion of PsP, because surgery would be considered more appropriate for PD than for PsP.

While the calculated sensitivity for DSC perfusion in the external validation dataset was lower than the reported pooled sensitivity (0.83 [95 % CI: 0.73–0.89]), the specificity was higher than the pooled specificity of 0.78 (95 % CI: 0.65–0.88). Particularly the number of false-negatives was slightly higher in our validation cohort, resulting in lower sensitivity values (between 0.47 and 0.77). This finding has implications for clinical practice, because this would result in patients with PD being falsely classified as having PsP, for whom follow-up with MRI or systemic anti-tumor therapy would be continued unnecessarily, with potentially detrimental consequences. This finding also exemplifies the need for external validation of study results in independent datasets, to better define the reliability of the imaging results with the different techniques.

In conclusion, this meta-analysis shows the highest pooled sensitivity and specificity when combining perfusion and diffusion MRI to differentiate between PD and PsP in brain metastasis patients during follow-up after focal high dose radiation therapy. Despite the limitations of the studies included in this meta-analysis, the pooled sensitivity and specificity of all MRI techniques are important results in optimising treatment evaluation for brain metastasis. For future research we would suggest using larger cohorts investigating the diagnostic accuracy for combined MRI techniques. As there is a lot of heterogeneity of the reviewed studies regarding imaging protocols and follow-up methods, we encourage harmonization of imaging protocols [6] and also systematic reporting of treatment response within international collaborations. We would also suggest using predefined cut-offs to prevent a high risk of bias in the index test domain, or to externally validate any newly defined cut-off values. Lastly, we would suggest research on the use of ASL perfusion MRI.

Declaration of Competing Interest

The authors declare that they have no known competing financial interests or personal relationships that could have appeared to influence the work reported in this paper.

Acknowledgements

The authors wish to thank the Erasmus MC medical library for their excellent support. This research was funded by "Leading the Change" (80-85009-98-2008-NVvR).

Guarantor

The scientific guarantor of this publication is dr. Anouk van der Hoorn.

The authors of this manuscript declare no relationships with any companies, whose products or services may be related to the subject matter of the article.

Statistics and Biometry

Jeremy Labrecque kindly provided statistical advice for this manuscript.

No complex statistical methods were necessary for this paper.

Informed Consent

Only if the study is on human subjects:

Written informed consent was obtained from all subjects (patients) in this study, if still alive during the study (validation cohort).

Written informed consent was not required for this study because some patients were deceased at the time of this study, so no informed consent was possible (validation cohort).

Only if the study is on animals:

Approval from the institutional animal care committee was obtained. (not applicable).

Ethical Approval

Institutional Review Board approval was obtained (for independent validation cohort).

Study subjects or cohorts overlap

Some study subjects or cohorts have been previously reported: An independent cohort was used for external validation. 16 of the 39 patients used for this cohort have been studied in another study which is published in https://doi.org/10.3389/fonc.2022.849657 Frontiers Oncology. That study has a different aim (comparison between ASL and DSC perfusion), so we do not indicate this as overlap.

Methodology

- prospective and retrospective (differs per included study, validation cohort retrospective).
- meta-analysis (with independent validation cohort).
- performed at one institution.

Appendix A. Supplementary material

Supplementary data to this article can be found online at https://doi.org/10.1016/j.radonc.2022.10.026.

References

[1] Lamba N, Wen PY, Aizer AA. Epidemiology of brain metastases and leptomeningeal disease. Neuro Oncol 2021.
[2] Beg U et al. Current Landscape and Future Prospects of Radiation Sensitizers for Malignant Brain Tumors: A Systematic Review. World Neurosurg; 2021.

[3] Thust SC, van den Bent MJ, Smits M. Pseudoprogression of brain tumors. J Magn Reson Imaging 2018.
[4] Stockham AL et al. Conventional MRI does not reliably distinguish radiation necrosis from tumor recurrence after stereotactic radiosurgery. J Neurooncol 2012;109:149–58.
[5] Kwee RM, Kwee TC. Dynamic susceptibility MR perfusion in diagnosing recurrent brain metastases after radiotherapy: a systematic review and meta-analysis. J Magn Reson Imaging 2020;51:524–34.
[6] Thust SC et al. Glioma imaging in Europe: a survey of 220 centres and recommendations for best clinical practice. Eur Radiol 2018;28:3306–17.
[7] van Dijken BRJ et al. Perfusion MRI in treatment evaluation of glioblastomas: clinical relevance of current and future techniques. J Magn Reson Imaging 2019;49:11–22.
[8] Moher D et al. Preferred reporting items for systematic reviews and meta-analyses: the PRISMA statement. BMJ 2009;339.
[9] Shea BJ et al. AMSTAR is a reliable and valid measurement tool to assess the methodological quality of systematic reviews. J Clin Epidemiol 2009;62:1013–20.
[10] Whiting PF et al. QUADAS-2: a revised tool for the quality assessment of diagnostic accuracy studies. Ann Internal Med 2011;155:529–36.
[11] Shim SR, Kim SJ, Lee J. Diagnostic test accuracy: application and practice using R software. Epidemiol Health 2019;41:e2019007.
[12] Reitsma JB et al. Bivariate analysis of sensitivity and specificity produces informative summary measures in diagnostic reviews. J Clin Epidemiol 2005;58:982–90.
[13] Bodensohn R et al. Prospective validation trial of magnetic resonance imaging based contrast clearance analysis (cca) to differentiate between pseudoprogression/ radiation necrosis and progressive disease following cranial radiotherapy. Neuro-Oncol 2021;23:p. ii23.
[14] Chen X et al. External validation of a radiomics-based machine learning model for distinguishing radiation necrosis from progression of brain metastases treated with stereotactic radiosurgery. Int J Radiat Oncol Biol Phys 2020;108: e722–3.
[15] Chernov MF et al. Multivoxel proton MRS for differentiation of radiation-induced necrosis and tumor recurrence after gamma knife radiosurgery for brain metastases. Brain Tumor Pathol 2006;23:19–27.
[16] Dohm AE et al. Imaging-driven biophysical model for the differentiation of tumor progression from radiation necrosis. Int J Radiat Oncol Biol Phys 2019;105:S31.
[17] Mardor Y et al. Delayed contrast MRI for differentiating brain tumors from treatment effects in conventional and combined treatments. Int J Radiat Oncol Biol Phys 2015;93:S108–9.
[18] Mardor Y et al. Delayed contrast MRI: a new paradigm in neuro-oncology. J Clin Oncol 2014;32.
[19] Mehrabian H et al. Differentiation between radiation necrosis and tumor progression using chemical exchange saturation transfer. Clin Cancer Res 2017;23:3667–75.
[20] Morabito R et al. DCE and DSC perfusion MRI diagnostic accuracy in the follow-up of primary and metastatic intra-axial brain tumors treated by radiosurgery with cyberknife. Radiat Oncol 2019;14.
[21] Narang J et al. Differentiating treatment-induced necrosis from recurrent/ progressive brain tumor using nonmodel-based semiquantitative indices derived from dynamic contrast-enhanced T1-weighted MR perfusion. Neuro-Oncol 2011;13:1037–46.
[22] Peker S et al. The use of treatment response assessment maps in discriminating between radiation effect and persistent tumoral lesion in metastatic brain tumors treated with gamma knife radiosurgery. World Neurosurg 2021;146:e1134–46.
[23] Prasanna P et al. Disorder in pixel-level edge directions on T1Wi is associated with the degree of radiation necrosis in primary and metastatic brain tumors: preliminary findings. Am J Neuroradiol 2019;40:412–7.
[24] Sahgal A et al. MRI perfusion biomarkers predicting early response for brain metastasis treated with high-dose radiation therapy. Int J Radiat Oncol Biol Phys 2013;87:S270–1.
[25] Schlemmer HP et al. Proton MR spectroscopic evaluation of suspicious brain lesions after stereotactic radiotherapy. AJNR Am J Neuroradiol 2001;22:1316–24.
[26] Sparacia G et al. Value of serial magnetic resonance imaging in the assessment of brain metastases volume control during stereotactic radiosurgery. World J Radiol 2016;8:916–21.
[27] Tiwari P et al. Computer-extracted texture features to distinguish cerebral radionecrosis from recurrent brain tumors on multiparametric mri: a feasibility study. Am J Neuroradiol 2016;37:2231–6.
[28] Wagner S et al. Radiation injury versus malignancy after stereotactic radiosurgery for brain metastases: Impact of time-dependent changes in lesion morphology on MRI. Neuro-Oncol 2017;19:586–94.
[29] Barajas RF et al. Distinguishing recurrent intra-axial metastatic tumor from radiation necrosis following gamma knife radiosurgery using dynamic susceptibility-weighted contrast-enhanced perfusion MR imaging. Am J Neuroradiol 2009;30:367–72.
[30] Chernov M et al. Differentiation of the radiation-induced necrosis and tumor recurrence after gamma knife radiosurgery for brain metastases: importance of multi-voxel proton MRS. Minimally Invasive Neurosurg 2005;48:228–34.
[31] Choi YJ, Kim HS, Kim SJ. Bimodal histogram analysis of wash-in-Emax ratio: Dynamic contrast-enhanced perfusion MRI parameter in metastatic brain tumor after radiosurgery. Neuroradiology 2012;54:S66–7.
[32] Dequesada IM et al. Can standard magnetic resonance imaging reliably distinguish recurrent tumor from radiation necrosis after radiosurgery for brain metastases? a radiographic-pathological study. Neurosurgery 2008;63:898–903.
[33] Kim DY et al. Utility of intravoxel incoherent motion MR imaging for distinguishing recurrent metastatic tumor from treatment effect following gamma knife radiosurgery: Initial experience. Am J Neuroradiol 2014;35:2082–90.
[34] Koh MJ et al. Which is the best advanced MR imaging protocol for predicting recurrent metastatic brain tumor following gamma-knife radiosurgery: focused on perfusion method. Neuroradiology 2015.
[35] Lai G et al. Diagnostic accuracy of PET, SPECT, and arterial spin-labeling in differentiating tumor recurrence from necrosis in cerebral metastasis after stereotactic radiosurgery. Am J Neuroradiol 2015;36:2250–5.
[36] Narloch JL et al. Biopsy of enlarging lesions after stereotactic radiosurgery for brain metastases frequently reveals radiation necrosis. Neuro-Oncol 2017;19:1391–7.
[37] Tomura N et al. Differentiation between treatment-induced necrosis and recurrent tumors in patients with metastatic brain tumors: Comparison among 11C-Methionine-PET, FDG-PET, MR permeability imaging, and MRI-ADC-preliminary results. Am J Neuroradiol 2017;38:1520–7.
[38] Truong MT et al. Results of surgical resection for progression of brain metastases previously treated by gamma knife radiosurgery. Neurosurgery 2006;59:86–95.
[39] Wang B et al. Postcontrast T1 mapping for differential diagnosis of recurrence and radionecrosis after gamma knife radiosurgery for brain metastasis. Am J Neuroradiol 2018;39:1025–31.
[40] Correa, R., et al., *"Lesion-habitat" Radiomics to distinguish Radiation Necrosis From Tumor Recurrence on post-treatment MRI in Metastatic Brain Tumors.* 2020. **11314**.
[41] Cicone F et al. Accuracy of F-DOPA PET and perfusion-MRI for differentiating radionecrotic from progressive brain metastases after radiosurgery. Eur J Nucl Med Mol Imaging 2015;42:103–11.
[42] Detsky JS et al. Differentiating radiation necrosis from tumor progression in brain metastases treated with stereotactic radiotherapy: utility of intravoxel incoherent motion perfusion MRI and correlation with histopathology. J Neuro-Oncol 2017;134:433–41.
[43] Hatzoglou V et al. A prospective trial of dynamic contrast-enhanced MRI perfusion and fluorine-18 FDG PET-CT in differentiating brain tumor progression from radiation injury after cranial irradiation. Neuro-Oncol 2016;18:873–80.
[44] Kano H et al. T1/T2 matching to differentiate tumor growth from radiation effects after stereotactic radiosurgery. Neurosurgery 2010;66:486–91.
[45] Leeman JE et al. Extent of perilesional edema differentiates radionecrosis from tumor recurrence following stereotactic radiosurgery for brain metastases. Neuro-Oncol 2013;15:1732–8.
[46] Lohmann P et al. Combined FET PET/MRI radiomics differentiates radiation injury from recurrent brain metastasis. NeuroImage-Clin 2018;20:537–42.
[47] Muto M et al. Dynamic susceptibility contrast (DSC) perfusion MRI in differential diagnosis between radionecrosis and neoangiogenesis in cerebral metastases using rCBV, rCBF and K2. Radiol Med 2018;123:545–52.
[48] Dohm AE et al. Clinical assessment of a biophysical model for distinguishing tumor progression from radiation necrosis. Med Phys 2021;48:3852–9.
[49] Hainc, N., et al., *The centrally restricted diffusion sign on MRI for assessment of radiation necrosis in metastases treated with stereotactic radiosurgery.* 2021.
[50] Lee, D.H., et al., *Tumor habitat analysis by magnetic resonance imaging distinguishes tumor progression from radiation necrosis in brain metastases after stereotactic radiosurgery.* 2021.
[51] Travers S et al. Reliability of magnetic resonance spectroscopy and positron emission tomography computed tomography in differentiating metastatic brain tumor recurrence from radiation necrosis. World Neurosurg 2021;151: e1059–68.
[52] Otman H et al. Differential diagnosis between progression and radionecrosis in brain metastases after stereotactic radiosurgery using hybrid FDG-PET and MRI coregistered images. Med Nucl 2021;45:113–8.
[53] Hettal L et al. Radiomics method for the differential diagnosis of radionecrosis versus progression after fractionated stereotactic body radiotherapy for brain oligometastasis. Radiat Res 2020.
[54] Knitter JR et al. Interval change in diffusion and perfusion mri parameters for the assessment of pseudoprogression in cerebral metastases treated with stereotactic radiation. Am J Roentgenol 2018;211:168–75.
[55] Larroza A et al. Support vector machine classification of brain metastasis and radiation necrosis based on texture analysis in MRI. J Magn Reson Imaging 2015;42:1362–8.
[56] Peng L et al. Distinguishing true progression from radionecrosis after stereotactic radiation therapy for brain metastases with machine learning and radiomics. Int J Radiat Oncol Biol Phys 2018;102:1236–43.
[57] Cicone F et al. Long-term metabolic evolution of brain metastases with suspected radiation necrosis following stereotactic radiosurgery: longitudinal assessment by F-DOPA PET. Neuro-Oncol 2021;23:1024–34.
[58] Hoefnagels FWA et al. Radiological progression of cerebral metastases after radiosurgery: Assessment of perfusion MRI for differentiating between necrosis and recurrence. J Neurol 2009;256:878–87.
[59] Huang J et al. Differentiation between intra-axial metastatic tumor progression and radiation injury following fractionated radiation therapy or stereotactic radiosurgery using MR spectroscopy, perfusion MR imaging or volume progression modeling. Magn Reson Imaging 2011;29:993–1001.

[60] Sawlani V et al. Evaluation of response to stereotactic radiosurgery in brain metastases using multiparametric magnetic resonance imaging and a review of the literature. Clin Oncol 2019;31:41–9.
[61] Zhang Z et al. A predictive model for distinguishing radiation necrosis from tumour progression after gamma knife radiosurgery based on radiomic features from MR images. Eur Radiol 2018;28:2255–63.
[62] Cha J et al. Analysis of the layering pattern of the apparent diffusion coefficient (ADC) for differentiation of radiation necrosis from tumour progression. Eur Radiol 2013;23:879–86.
[63] Wang B et al. Absolute CBV for the differentiation of recurrence and radionecrosis of brain metastases after gamma knife radiotherapy: a comparison with relative CBV. Clin Radiol 2018;73:758.e1–7.
[64] Mitsuya K et al. Perfusion weighted magnetic resonance imaging to distinguish the recurrence of metastatic brain tumors from radiation necrosis after stereotactic radiosurgery. J Neuro-Oncol 2010;99:81–8.
[65] van Dijken BRJ et al. Diagnostic accuracy of magnetic resonance imaging techniques for treatment response evaluation in patients with high-grade glioma, a systematic review and meta-analysis. Eur Radiol 2017;27:4129–44.
[66] Jovanovic M et al. Differentiation between progression and pseudoprogresion by arterial spin labeling MRI in patients with glioblastoma multiforme. J Buon 2017;22:1061–7.
[67] Ferre JC et al. Arterial spin labeling (ASL) Perfusion: techniques and clinical use. J Radiol Diagno Intervent 2013;94:1208–21.
[68] Galldiks N et al. PET imaging in patients with brain metastasis-report of the RANO/PET group. Neuro Oncol 2019;21:585–95.
[69] Kerkhof M et al. Clinical applicability of and changes in perfusion MR imaging in brain metastases after stereotactic radiotherapy. J Neurooncol 2018;138:133–9.